processes

MDPI

Article

A Damage Identification Method Based on Minimum Mean Square Error Estimation for Wind Tunnel Flexible Plate Condition Monitoring System

Kang Yun [1,2], Mingyao Liu [1,*], Jingliang Wang [1] and Cong Li [1]

[1] School of Mechanical and Electronic Engineering, Wuhan University of Technology, Wuhan 430070, China; yunkang@whut.edu.cn (K.Y.)
[2] Henan Key Laboratory of Intelligent Manufacturing of Mechanical Equipment, College of Mechanical and Electrical Engineering, Zhengzhou University of Light Industry, Zhengzhou 450002, China
* Correspondence: myliu@whut.edu.cn; Tel.: +86-130-7120-2580

Abstract: In this paper, we propose a damage identification method based on minimum mean square error estimation for a wind tunnel flexible plate condition monitoring system. Critical structural members of important equipment are large in size, and the measurement systems used to monitor their condition are often complex. The proposed damage identification method is based on the minimum mean squared error estimator and the generalized likelihood ratio test. It introduced activation function to generate the standard deviation of the data, which can then simulate the sensor output. A single sensor damage only affects a single dimension of the output data matrix of the measurement system. However, structural damage affects the output of multiple sensors. The damage identification method proposed in this paper can not only distinguish the sensor damage from the structure damage, but also locate the damaged sensor or structure damage location. This method can identify the measurement system output anomalies caused by structural damage and locate the approximate location of the damage. It can be applied to damage identification of important structural members such as flexible wind tunnel plates. The damage identification method proposed in this paper is of great significance for damage identification and localization of key components and sensor systems.

Keywords: wind tunnel flexible plate; minimum mean square error estimation; generalized likelihood ratio test; damage identification

Citation: Yun, K.; Liu, M.; Wang, J.; Li, C. A Damage Identification Method Based on Minimum Mean Square Error Estimation for Wind Tunnel Flexible Plate Condition Monitoring System. *Processes* **2023**, *11*, 1791. https://doi.org/10.3390/pr11061791

Academic Editor: Vicenç Puig

Received: 27 March 2023
Revised: 25 May 2023
Accepted: 5 June 2023
Published: 12 June 2023

1. Introduction

The wind tunnel is an important piece of experimental equipment used for aerodynamic research. It is also the key experimental equipment for research on the aerodynamic layout of the aircraft. Several studies on the wind tunnel construction were carried out several decades previously [1–4]. For a long time, wind tunnels have provided the basis for aerodynamic experiments in various fields (Wind Tunnel Application) [5–10]. The flexible plate is the core component of the wind tunnel. It is the key to producing a stable flow field. Flexible plates are subjected to complex loads during the operation of the wind tunnel. Therefore, the health status of the flexible plate needs to be monitored in real time. The stress field is an important physical quantity that reflects the health status of the flexible plate. The flexible plate stress field requires multi-point measurements. Fiber Bragg gratings (FBG) are fiber optic sensors that are sensitive to stress and temperature. In this paper, the FBG sensor is used to measure the local strain of the flexible plate. The measurement system composed of multiple sensors will have measurement errors caused by the failure of individual sensors during operation.

The principal component analysis algorithm (PCA) is the most commonly used data dimensionality reduction method. It is widely used in data analysis, artificial intelligence

algorithms and other fields [11–20]. Previous research has established that principal component analysis is used to diagnose the damage of the sensor in the sensor system. Dunia has made use of PCA to develop a model that captures correlation among different sensors. That study reconstructed the sensor system with the help of the model and established a sensor fault diagnosis method [21]. A method for diagnosing sensor failures in air-handling units based on multivariate statistical methods and principal component analysis has been proposed [22]. Hu et al. proposed an adaptive principal component analysis method to train the sensor group data and used this method to identify the chiller sensor fault [23]. Navi et al. studied a partial kernel principal component analysis method to detect sensor faults in aeroderivative industrial gas turbines [24]. Sharifi and Langari proposed a probabilistic principal component analysis model for diagnosing sensor faults in nonlinear systems [25]. Li et al. constructed a principal component analysis method based on statistical methods and used it for sensor fault detection in nuclear power plants [26]. Guannan and Yunpeng proposed a principal component analysis method based on ensemble empirical mode decomposition denoising and applied it to sensor fault detection in heating, ventilating and air conditioning systems [27]. Yu et al. researched a corrected reconstruction algorithm to improve the accuracy of PCA reconstruction. In this study, the improved principal component analysis method is applied to the detection of sensor faults in nuclear power plants [28]. Shaomin et al. studied a principal component analysis method using the Euclidean distance statistical method to remove outliers and used it for sensor fault diagnosis in nuclear power plants [29]. These studies are applications of PCA methods in the field of process control such as chemical production. The number of sensors in these applications is limited and the measurement data are not abundant. However, for wind tunnel flexible plate condition monitoring system with multiple measurement parameters and sensors, the PCA method alone cannot handle the task.

There are many methods for diagnosing sensor faults besides PCA. Mohamed has submitted a model-based fault diagnosis method using knowledge base and fuzzy logic techniques [30]. Berriri and Slama-Belkhodja constructed an enhanced parity space approach to solve the problem of sensor fault detection and isolation [31]. Sharifi isolated sensor faults based on the residual's direction found from the residual generator [32]. Rao and Kasireddy submitted a sensor fault detection and isolation technique based on the null subspace method [33]. Yang et al. researched an online sensor fault identification method using the random forest algorithm [34]. Shahnazi and Qing developed a sensor fault identification method based on the adaptive fuzzy proportional-derivative sliding mode observer for nonlinear systems [35]. Yuqing et al. proposed a fault diagnosis algorithm based on the multi-sensor fusion method for sensor faults in spacecraft control systems [36]. Heydarzadeh and Nourani studied a novel fault detection and isolation architecture based on predictive models of fault-free processes [37]. Tolouei and Shoorehdeli built a sensor fault detection approach based on nonlinear parity technique [38]. Taken together, this research makes it known that the fault diagnosis of the sensor can start from many aspects.

The response of the sensor system can be used not only to diagnose sensor faults, but also to identify structural damage. Kullaa constructed a structural damage identification method based on the dynamic response of a series of accelerometers [39–42]. First, he estimated each sensor using minimum mean squared error estimation; second, he used a generalized likelihood ratio test to detect abnormal sensors; finally, he replaced the detected abnormal sensor response with the remaining sensor responses to distinguish structural damage from sensor fault.

The flexible plate is a key component of the wind tunnel. The premise of forming a stable flow field in a wind tunnel is the precise deformation of the flexible plate. During this process, the flexible plate must withstand the pushing force (traction) of the actuator and the aerodynamic load. Complex loads can cause damage to the flexible plate. Therefore, the health status of the flexible plate should be monitored.

In addition, the design life of flexible plate structures in wind tunnels often exceeds several decades, whereas fiber optic sensors, as an optical component, have a sensor life

of only ten years and are prone to failure due to aging during use. On the other hand, in flexible plate health monitoring systems, dense sensor arrays are usually arranged to achieve good monitoring and diagnostic performance. A sensor network composed of a large number of sensors operates online for a long time, and is affected by environmental factors such as temperature, humidity, vibration, impact, and changes in workload, resulting in performance degradation or even failure of some sensors. The structural response changes caused by sensor failures are often on the same order of magnitude as the structural response changes caused by structural damage, and are often mistakenly attributed to structural damage, leading to system false positives. Therefore, it is of great importance to study sensor fault detection and identification in structural health monitoring of flexible plates.

The health status monitoring system of the wind tunnel flexible plate is shown in Figure 1. The optimal layout of sensor networks has physical model redundancy and statistical related redundancy characteristics. Thus, the output of a single faulty sensor in the network can be reconstructed from the remaining health sensors to achieve fault tolerance monitoring. The damage identification method proposed in this paper can not only distinguish the sensor damage from the structure damage, but also locate the damaged sensor or structure damage location. A single sensor damage only affects a single dimension of the output data matrix of the measurement system. Therefore, the measurement data of the damaged sensor can be replaced by that of other health sensors. The results of simulation experiments confirm this analysis. When the structure itself is damaged, the output model of the sensor network no longer obeys the Gaussian process; thus, sensor data near healthy structures cannot be used as a substitute for sensor data near structural damage. The experimental results show that the change in evaluation indicator caused by structural damage will not disappear because the damage location sensor data are replaced. Moreover, the experimental results show that the damage detection method proposed in this paper can locate the damaged sensor or structure damage location. The damage identification method proposed in this paper can not only distinguish the sensor damage from the structure damage, but also locate the damaged sensor or structure damage location. This method can identify the measurement system output anomalies caused by structural damage and locate the approximate location of the damage. This paper is a meaningful attempt to apply the method to the health condition monitoring of wind tunnel flexible plates. The major structure of this study takes the form of four parts, including Sections 2–4.

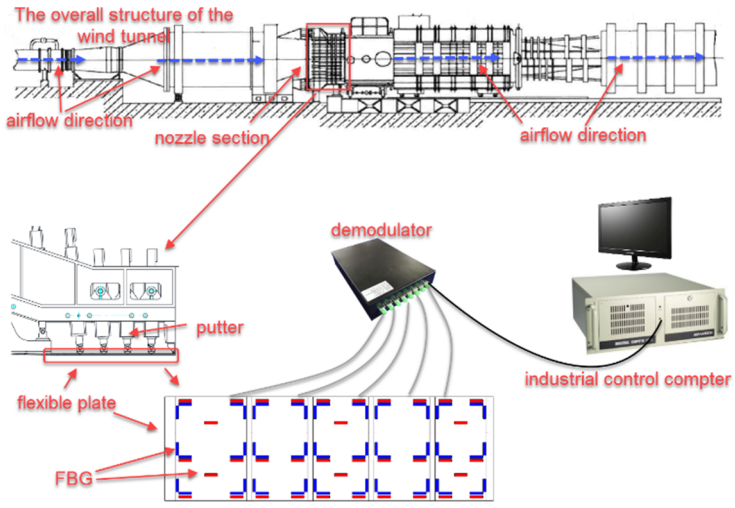

Figure 1. Health status monitoring system of wind tunnel flexible plate.

2. Structural Damage and Sensor Fault Detection Method

Structural damage and degradation of sensor performance can cause changes in the detected sensor system output values. This section uses statistical analysis methods to

detect the abnormal output of sensor systems. The analysis methods used in this paper are: minimum mean square error estimator (MMSE) and generalized likelihood ratio test (GLRT).

2.1. Minimum Mean Square Error Estimator

The output model of the sensor network conforms to a Gaussian process. When the sample (Change with Time) size is large enough, the output of the sensor system obeys a multivariate normal distribution.

$$p(\mathbf{x}) = |2\pi\boldsymbol{\Sigma}|^{-1/2} \exp\left[-\frac{1}{2}(\mathbf{x}-\boldsymbol{\mu})^T \boldsymbol{\Sigma}^{-1}(\mathbf{x}-\boldsymbol{\mu})\right] \tag{1}$$

In the above Equation (1), $\mathbf{X}$ represents the output vector of the sensor system at the same time; $\boldsymbol{\mu}$ is the sample mean vector; $\boldsymbol{\Sigma}$ is the covariance matrix.

Any one sensor is assumed to be abnormal, then the rest of the sensors can represent it. The abnormal output of sensor system is u, then the output vector of the remaining sensors is $\mathbf{v}$. The sensor network input vector can be expressed as:

$$\mathbf{x} = \begin{bmatrix} u \\ \mathbf{v} \end{bmatrix} \tag{2}$$

Next, the covariance matrix can be expressed as:

$$\boldsymbol{\Sigma} = \begin{bmatrix} \boldsymbol{\Sigma}_{uu} & \boldsymbol{\Sigma}_{uv} \\ \boldsymbol{\Sigma}_{vu} & \boldsymbol{\Sigma}_{vv} \end{bmatrix} = \begin{bmatrix} \boldsymbol{\Gamma}_{uu} & \boldsymbol{\Gamma}_{uv} \\ \boldsymbol{\Gamma}_{vu} & \boldsymbol{\Gamma}_{vv} \end{bmatrix}^{-1} = \boldsymbol{\Gamma}^{-1} \tag{3}$$

Then, the abnormal output of sensor system can be estimated as:

$$\hat{u} = E(u|\mathbf{v}) = \mu_u - \boldsymbol{\Gamma}_{uu}^{-1}\boldsymbol{\Gamma}_{uv}(\mathbf{v}-\boldsymbol{\mu}_v) \tag{4}$$

where μ_u is the abnormal sensor output average; $\boldsymbol{\mu}_v$ is the normal sensor output average. $E(u \mid \mathbf{v})$ represents expectation. The error covariance matrix is

$$\boldsymbol{\Phi} = \mathrm{cov}(u\Big|\mathbf{v}) = \boldsymbol{\Gamma}_{uu}^{-1} \tag{5}$$

The expectation and covariance matrix calculated by Equations (4) and (5) are intermediate quantities of Equation (1).

2.2. Sensor System Abnormal Output Detection Generalized Likelihood Ratio Test (GLRT)

The estimated value of the anomaly sensor follows Gaussian distribution (Conditional Probability):

$$p(u|\mathbf{v}) = |2\pi\boldsymbol{\Phi}|^{-1/2} \exp\left[-\frac{1}{2}(u-\hat{u})^T \boldsymbol{\Phi}^{-1}(u-\hat{u})\right] \tag{6}$$

The abnormal output of sensor system is confirmed by hypothesis testing. The generalized likelihood ratio for each sample is as follows:

$$L = \frac{p(u|\mathbf{v}; H_1)}{p(u|\mathbf{v}; H_0)} \tag{7}$$

where $p(u \mid \mathbf{v};H_i)$ is conditional probability density function for the H_i hypothesis; H_1 is alternative hypothesis; H_0 is null hypothesis. In order to effectively detect the abnormal output of the sensor system, the above ratios are processed:

$$s = \ln(L) = \ln \frac{p(u|\mathbf{v}; H_1)}{p(u|\mathbf{v}; H_0)} \tag{8}$$

The generalized likelihood ratio matrix of the whole sample is:

$$\mathbf{S} = \begin{bmatrix} s_{11} & s_{12} & \cdots & s_{1n} \\ s_{21} & s_{22} & \cdots & s_{2n} \\ \vdots & \vdots & \vdots & \vdots \\ s_{m1} & s_{m2} & \cdots & s_{mn} \end{bmatrix} \tag{9}$$

where s_{ij} is generalized likelihood ratio for the i-th sample of the j-th sensor. Overall, if a sensor has a large, generalized likelihood ratio, it is likely to generate anomalous output. In order to determine the source of abnormal output, the root mean square (RMS) of each sensor (j = 1, 2, 3, . . . , n) is calculated separately:

$$\overline{s}_j = \frac{1}{m}\sqrt{\sum_{i=1}^{m} s_{ij}^2} \tag{10}$$

If the RMS of one sensor is larger than that of the other sensors and the difference is significant, then it is the sensor that is producing abnormal output.

2.3. Principal Component Analysis (PCA)

For a sensor system, it has multiple sensors, so it has multi-dimensional data output. For the evaluation of multidimensional data, dimensionality reduction is generally adopted. The PCA is the most commonly used data dimensionality reduction method. In order to find a quantity that reflects the generalized likelihood ratio level of the sensor system at each sample moment, a PCA analysis is performed on the matrix **S**.

First, the number of samples for PCA analysis is set to p, and the matrix **S** is divided into l ($l = m/p$) groups.

$$\mathbf{S} = \left[\begin{array}{cccc} s_{1,1} & s_{1,2} & \cdots & s_{1,n} \\ s_{2,1} & s_{2,2} & \cdots & s_{2,n} \\ \vdots & \vdots & \vdots & \vdots \\ s_{p,1} & s_{p,2} & \cdots & s_{p,n} \\ \hdashline s_{p+1,1} & s_{p+1,2} & \cdots & s_{p+1,n} \\ s_{p+2,1} & s_{p+2,2} & \cdots & s_{p+2,n} \\ \vdots & \vdots & \vdots & \vdots \\ s_{2p,1} & s_{2p,2} & \cdots & s_{2p,n} \\ \hdashline \vdots & \vdots & \vdots & \vdots \\ \hdashline s_{m-p+1,1} & s_{m-p+1,2} & \cdots & s_{m-p+1,n} \\ s_{m-p+2,1} & s_{m-p+2,2} & \cdots & s_{m-p+2,n} \\ \vdots & \vdots & \vdots & \vdots \\ s_{m,1} & s_{m,2} & \cdots & s_{m,n} \end{array}\right] = \begin{bmatrix} \mathbf{G}_1 \\ \mathbf{G}_2 \\ \vdots \\ \mathbf{G}_l \end{bmatrix} \tag{11}$$

After PCA analysis, the first principal component score $\boldsymbol{gs}_i = (gs_{i1}, gs_{i2}, \ldots, gs_{in})$ of the matrix $\mathbf{G}_\mathrm{i}$ (i = 1, 2, . . . , l) is obtained. Then, the first principal component score matrix can be obtained:

$$\mathbf{GS} = \begin{bmatrix} gs_{11} & gs_{12} & \cdots & gs_{1n} \\ gs_{21} & gs_{22} & \cdots & gs_{2n} \\ \vdots & \vdots & \vdots & \vdots \\ gs_{l1} & gs_{l2} & \cdots & gs_{ln} \end{bmatrix} \tag{12}$$

The first principal component score of matrix $\mathbf{G}_i$ is an important parameter reflecting the level of the data in this group. In order to fully reflect the situation of matrix $\mathbf{G}_i$, this

paper selects the maximum (high-indicator) (α_i) and minimum (low-indicator) (β_i) scores of its first principal component as evaluation indicators. The indicator matrixes are:

$$\begin{cases} A = \begin{bmatrix} \alpha_1 & \alpha_2 & \cdots & \alpha_l \end{bmatrix}^T \\ B = \begin{bmatrix} \beta_1 & \beta_2 & \cdots & \beta_l \end{bmatrix}^T \end{cases} \tag{13}$$

2.4. Statistical Process Control (SPC)

Statistical process control is a process control tool that combines mathematics statistics. In this paper, the output data state of the sensor system is judged by the control chart. The key parameters of a control chart are the upper bound (*UCL*) and lower bound (*LCL*) of the indicator. Assume the indicator matrix is:

$$\mathbf{X} = \begin{bmatrix} x_1 & x_2 & \cdots & x_l \end{bmatrix}^T \tag{14}$$

The matrix **X** is divided into N ($N = l/q$) groups.

$$\begin{cases} \mathbf{X} = \begin{bmatrix} \boldsymbol{\gamma}_1 & \boldsymbol{\gamma}_2 & \cdots & \boldsymbol{\gamma}_N \end{bmatrix}^T \\ \boldsymbol{\gamma}_1 = \begin{bmatrix} x_1 & x_2 & \cdots & x_q \end{bmatrix} \\ \boldsymbol{\gamma}_2 = \begin{bmatrix} x_{q+1} & x_{q+2} & \cdots & x_{2q} \end{bmatrix} \\ \boldsymbol{\gamma}_q = \begin{bmatrix} x_{l-q+1} & x_{l-q+2} & \cdots & x_l \end{bmatrix} \end{cases} \tag{15}$$

The mean (K_j) and range (R_j) of the matrix $\boldsymbol{\gamma}_j$ (j = 1, 2, . . . , N) can be calculated as follows:

$$\begin{cases} K_j = \frac{1}{q} \sum\limits_{i=(j-1)q+1}^{jq} x_i \\ R_j = Max(\boldsymbol{\gamma}_j) - Min(\boldsymbol{\gamma}_j) \end{cases} \tag{16}$$

The upper limit (*UCL*) and lower limit (*LCL*) of the statistical quality control chart are solved using the following formula.

$$\begin{cases} UCL = \frac{1}{n} \sum\limits_{j=1}^{n} K_j + A_2 \frac{1}{n} \sum\limits_{j=1}^{n} R_j \\ LCL = \frac{1}{n} \sum\limits_{j=1}^{n} K_j - A_2 \frac{1}{n} \sum\limits_{j=1}^{n} R_j \end{cases} \tag{17}$$

where the value of A_2 is related to the sample size (q).

2.5. Detection Method

The indicator matrices **A** and **B** reflect the state of the sensor system output in the corresponding period. After the indicator matrices are calculated, this paper draws a control chart of the sensor system principal component scores. In the control chart, it can be displayed whether the principal component score of the sensor system output exceeds the limit.

3. Simulation Validation and Discussion

In this paper, the local acceleration information of the flexible plate is collected by simulation method. The details of the experiment are shown in Figure 2. As shown in the figure, one end of the flexible plate is fixed, and the impact load is loaded at the other end. The grid of the flexible plate is independently selected by the software. In this paper, acceleration measurement points are set locally on the flexible plate. The dynamic loads are then loaded onto the flexible plate. In this paper, local acceleration dynamic data of the flexible plate are collected under the healthy condition. Statistical regularity of acceleration data at each measurement point under structural health state is shown in Figure 3. The same experimental procedure was performed after the flexible plate structure was damaged.

The statistical rule of acceleration data for each measured point under structural damage is shown in Figure 4.

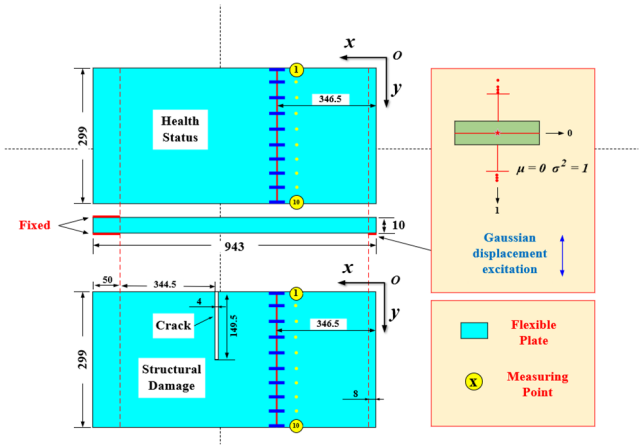

Figure 2. Schematic diagram of the simulation experiment.

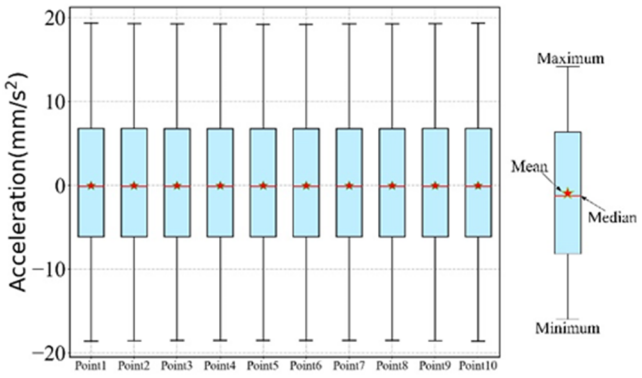

Figure 3. Statistical regularity of acceleration data at each measurement point under structural health state.

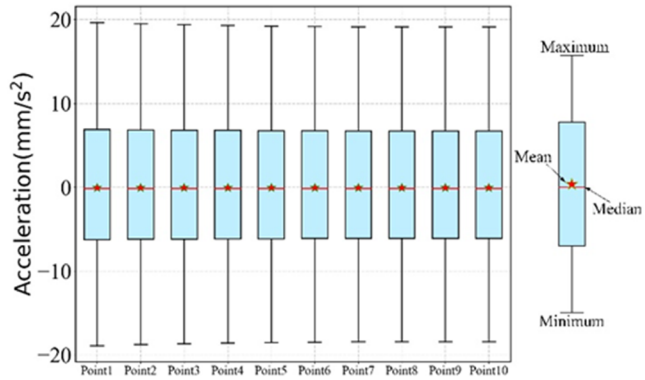

Figure 4. Statistical regularity of acceleration data for each measured point under structural damage.

As shown in Figures 3 and 4, the boxplots of each acceleration measurement point data for the healthy and damaged flexible plate are symmetrical and their mean and median values overlap. Therefore, it can be concluded that the acceleration measurement point data in both states follows the normal distribution. This conclusion provides the foundation for the simulation of acceleration data. In this paper, the reliability of the new damage identification method is verified by using sensor damage data and data from damaged structures, respectively. Both structural damage and data from damaged structure

were simulated from the data obtained from the previous simulation experiments. The acceleration data of the local measurement points of the flexible plate under two different conditions are examined under the normal distribution law. Assume that the mean and standard deviation of each measured point data for the health state and the state to be detected are: μ0, σ0, μ1, σ1. A new random number with normal distribution is generated to replace the simulated acceleration data. The formula for calculating the simulated acceleration random number is shown in Equation (22) to improve the sensitivity of this method, the standard deviation of the acceleration data in unknown state is processed. The formula for calculating standard deviation of measured points to be detected is shown in Equation (23). The formula for generating acceleration data for measured points in healthy and undetected states is shown in Equation (24).

$$\boldsymbol{\mu}^0 = \begin{bmatrix} \mu_1^0 & \mu_2^0 & \mu_3^0 & \cdots & \mu_{10}^0 \end{bmatrix} \tag{18}$$

$$\boldsymbol{\sigma}^0 = \begin{bmatrix} \sigma_1^0 & \sigma_2^0 & \sigma_3^0 & \cdots & \sigma_{10}^0 \end{bmatrix} \tag{19}$$

$$\boldsymbol{\mu}^1 = \begin{bmatrix} \mu_1^1 & \mu_2^1 & \mu_3^1 & \cdots & \mu_{10}^1 \end{bmatrix} \tag{20}$$

$$\boldsymbol{\sigma}^1 = \begin{bmatrix} \sigma_1^1 & \sigma_2^1 & \sigma_3^1 & \cdots & \sigma_{10}^1 \end{bmatrix} \tag{21}$$

$$\begin{cases} \mathbf{a} = \begin{bmatrix} a_1 & a_2 & a_3 & \cdots & a_{10} \end{bmatrix} \\ a_i = Norm(rand(), \mu_i, \sigma_i) \end{cases} \tag{22}$$

$$\begin{cases} \boldsymbol{\sigma}^* = \begin{bmatrix} \sigma_1^* & \sigma_2^* & \sigma_3^* & \cdots & \sigma_{10}^* \end{bmatrix} \\ \sigma_i^* = \sigma_i^1 + \frac{50\left(\sigma_i^1 - \sigma_i^0\right)}{1+e^{-100(\sigma_i^1 - \sigma_i^0)}} \end{cases} \tag{23}$$

$$\begin{cases} \mathbf{a}^0 = \begin{bmatrix} a_1^0 & a_2^0 & a_3^0 & \cdots & a_{10}^0 \end{bmatrix} \\ \mathbf{a}^1 = \begin{bmatrix} a_1^1 & a_2^1 & a_3^1 & \cdots & a_{10}^1 \end{bmatrix} \\ a_i^0 = Norm(rand(), \mu_i^0, \sigma_i^0) \\ a_i^1 = Norm(rand(), \mu_i^1, \sigma_i^*) \end{cases} \tag{24}$$

Based on the results of the simulation calculation of the flexible plate, the data of each measured point in the healthy state are extracted, and the mean ($\boldsymbol{\mu}^0$) and standard deviation ($\boldsymbol{\sigma}^0$) are calculated. The mean and standard deviation of each measured point data under the condition of flexible plate damage are: $\boldsymbol{\mu}^1$, $\boldsymbol{\sigma}^1$. The authors substituted the mean $\boldsymbol{\mu}^0$ and standard deviation $\boldsymbol{\sigma}^0$ of each measured point in the healthy state into Equation (24) to generate 2000 groups of simulated acceleration data as health data. The acceleration data of each test point after the flexible plate structure damage comprise 2000 groups. The first 1000 groups are generated with the mean and standard deviation in the healthy state, and the last 1000 groups are calculated with the mean $\boldsymbol{\mu}^1$ and standard deviation $\boldsymbol{\sigma}^*$ of each test point data in the structure damage state. To verify the effectiveness of this method in the case of sensor damage, the authors used the above methods to generate health and damage data. The mean and standard deviation used in the last 1000 sets of damage data are: $\boldsymbol{\mu}^1$, $\boldsymbol{\sigma}^\#$.

$$\begin{cases} \boldsymbol{\sigma}^\# = \begin{bmatrix} \sigma_1^\# & \sigma_2^\# & \sigma_3^\# & \cdots & \sigma_{10}^\# \end{bmatrix} \\ \sigma_i^\# = \sigma_i^0 (i = 1, 2, 3, \cdots, 9) \\ \sigma_{10}^\# = \sigma_{10}^0 + \frac{50\Delta}{1+e^{-100\Delta}} \end{cases} \tag{25}$$

The author substitutes the simulated sensor damage data generated by the above methods into the proposed diagnostic method and draws a control chart. The generalized likelihood ratio matrix **S** can be used to locate damaged sensors or structural damage locations. Because of the large number of test data, the positioning matrix **E** is introduced for easy expression. See Equation (26) for the calculation formula of **E**. The identification

effect of the diagnosis method proposed in this paper for Sensor damage is shown in Figure 5. Figure 5b identifies the damaged sensor label (No. 10 sensor). The measurement results of damaged sensors can be replaced by the measurement results of other healthy sensors. Equation (4) can calculate the measurement results of the replaced sensor. The change in each indicator after the damaged sensor is replaced is shown in Figure 6. As mentioned above, the authors made the same treatment for the data of structural damage. The authors have drawn relevant figures, as shown in Figures 7–9.

$$\begin{cases} \mathbf{E} = \begin{bmatrix} e_{1,1} & e_{1,2} & \cdots & e_{1,10} \\ e_{2,1} & e_{2,2} & \cdots & e_{2,10} \\ \vdots & \vdots & \ddots & \vdots \\ e_{\tau,1} & e_{\tau,2} & \cdots & e_{\tau,10} \end{bmatrix} \\ e_{f,j} = \frac{1}{\kappa} \sum_{i=(f-1)\kappa+1}^{f\kappa} s_{i,j} (f = 1, 2, \cdots, \tau) \end{cases} \tag{26}$$

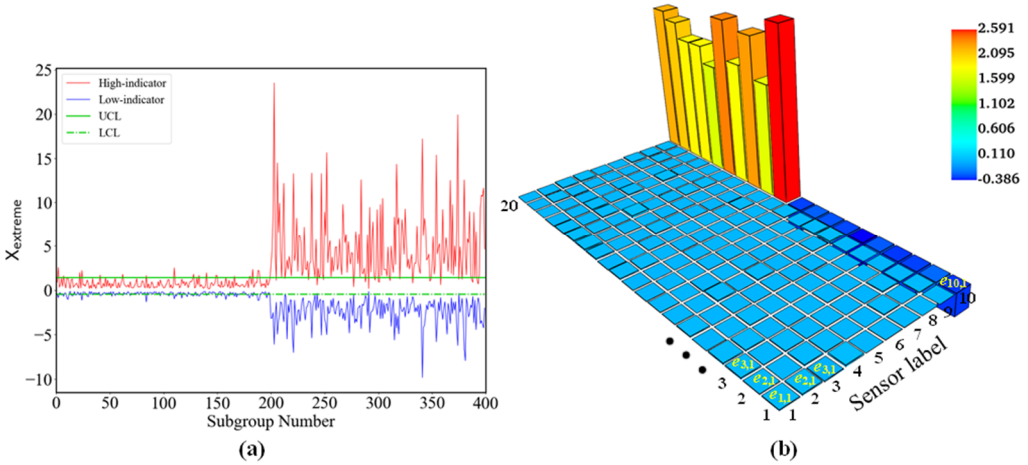

Figure 5. Identification effect of sensor damage. (**a**) Change in evaluation indicator for sensor damage. (**b**) Damage location matrix **E**.

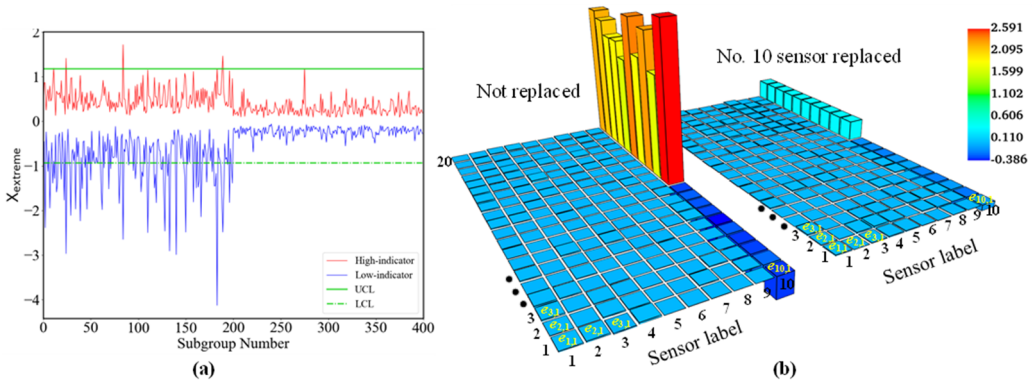

Figure 6. The evaluation indicator after the damaged sensor is replaced. (**a**) Change in evaluation indicator for sensor damage. (**b**) Damage location matrix **E**.

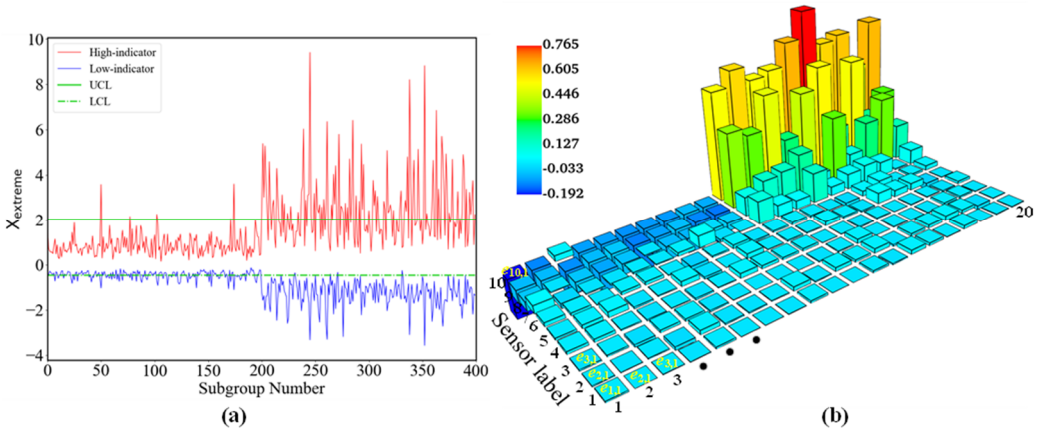

Figure 7. Identification effect of structural damage. (**a**) Change in evaluation indicator for structural damage. (**b**) Damage location matrix **E**.

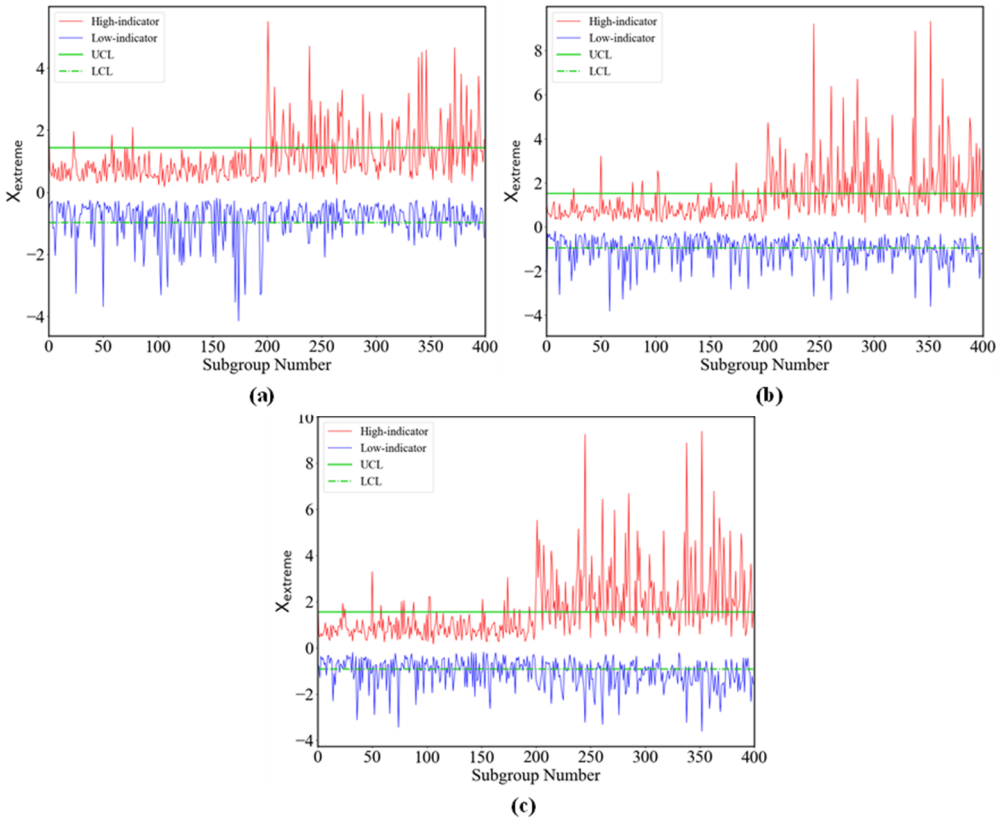

Figure 8. The evaluation indicator after the sensor near the structural damage is replaced. (**a**) No. 1 sensor is replaced. (**b**) No. 2 sensor is replaced. (**c**) No. 3 sensor is replaced.

This section simulates the dynamic acceleration data of the flexible plate and the sensor damage data. The authors input the sensor damage data and structural damage data into the damage identification method, and draw the correlation diagram. Figures 5 and 6 show that this method can identify and locate sensor damage. The reason is that the sensor damage only affects the single dimension of the system output data matrix. This effect can be eliminated by the rest of the healthy sensor data. Figures 7–9 show that this method can identify structural damage and locate the approximate location of damage. When the structure is damaged, the output model of the sensor network no longer conforms to the Gaussian process. Therefore, replacing the sensor data near the damage with the sensor data near the healthy structure will not change the deviation of the evaluation

indicator. Based on the original data, this paper generates health data and damage data that conform to the normal distribution law, which is a strong support to optimize the effect of damage identification methods. At the same time, the activation function (Equation (23)) is used to generate the standard deviation of the data to be measured, which amplifies the output deviation of the sensor system caused by damage. Therefore, the effect of damage identification is obvious.

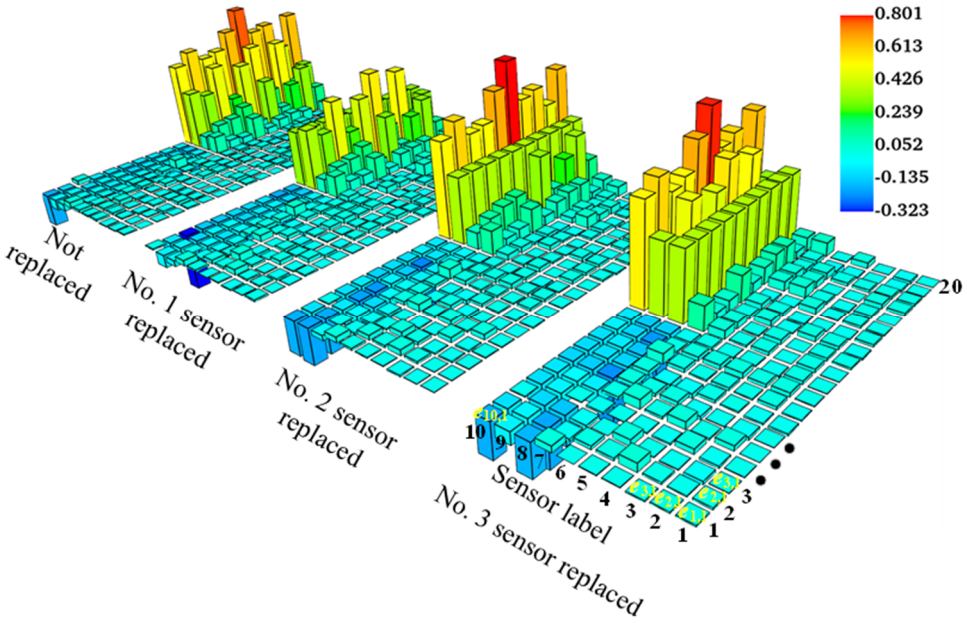

Figure 9. The location matrix **E** after the sensor near the structural damage is replaced.

4. Conclusions

In this paper, a damage identification method for the wind tunnel flexible plate based on minimum mean square error estimation is proposed. This method can effectively distinguish the sensor damage and structural damage, and can locate the damaged sensor and structural damage area. The following conclusions were drawn during the study:

(1) The damage identification method proposed in this paper can identify the output anomalies of the measurement system caused by sensor failures and locate the damaged sensors. The reason is that the sensor damage only affects a single dimension of the system output data matrix.

For a sensing system consisting of multiple sensors, each sensor inside it has output data. Individual sensor damage can cause a deviation in one dimension of the system output data. Additionally, the output model of the sensing network is consistent with the Gaussian process. In the case of data abundance, one dimension of the output data of the sensing network can be replaced by the data of the remaining dimensions. If the one dimension of the data deviates, then it can be simulated using the data from the remaining dimensions. For a sensing network with one sensor damage, a significant change in one dimension of the damage localization matrix occurs. If the abnormality disappears after one dimension of the damage localization matrix is replaced by the remaining dimensions, then the sensor of the abnormal dimension is the damage sensor.

(2) This method can identify the measurement system output anomalies caused by structural damage and locate the approximate location of the damage. The reason is that structural damage causes abnormal output of many sensors around it.

For the damaged structure, its inherent properties change. The excitation will cause the output of the sensor network to deviate because of its structural change. Structural damage can cause abnormal output of some sensors in the sensor network. These anomalies are caused by structural factors. The abnormal output caused by the internal causes of the structure cannot be simulated by the data of the health dimension. When the abnormality

of the damage location matrix cannot be simulated by the health dimension, the damage is caused by structural damage. The area where the abnormal output sensors are located is the damage location.

(3) The damage identification method proposed in this paper can be applied to damage identification of important structural members such as wind tunnel flexible plates. This is also an important contribution of this paper.

The flexible plate is a key component of the wind tunnel. Complex loads can cause damage to the flexible plate. Therefore, the health status of the flexible plate should be monitored. The health status of the flexible plate monitoring system consists of a number of FBG sensors arranged on it. The sensor damage of this system and the localization of the damaged sensor can be implemented using the method proposed in this paper. At the same time, the damage and damage location of the flexible plate can also be realized using this method.

(4) For a measurement system whose output data conform to the law of normal distribution, damage identification can be carried out using simulation data based on the original data.

For the measurement system whose output conforms to the Gaussian process, this method can be used to verify the effectiveness of the measurement system for damage identification in the absence of actual measurement data. At the same time, the method can provide a preview for the placement of the sensor network.

Author Contributions: Conceptualization, K.Y. and M.L.; methodology, K.Y.; software, K.Y.; validation, K.Y., J.W. and C.L.; formal analysis, K.Y.; investigation, K.Y.; resources, K.Y.; data curation, J.W.; writing—original draft preparation, K.Y.; writing—review and editing, K.Y.; visualization, K.Y.; supervision, K.Y.; project administration, K.Y.; funding acquisition, M.L. All authors have read and agreed to the published version of the manuscript.

Funding: This research was funded by the National Natural Science Foundation of China (General Program, No. 51375359).

Data Availability Statement: The data supporting the findings of this study are available within the article.

Conflicts of Interest: The authors declare no conflict of interest.

References

1. Erdmann, S.F. A new economic flexible nozzle for supersonic wind tunnels. *J. Aircr.* **1971**, *8*, 58–60. [CrossRef]
2. Erickson, L.L.; Kassner, D.L.; Guist, L.R. Investigation of Flexible Nozzle Wall-Flutter Incidents in the NASA-Ames Research Center 11- by 11-foot Transonic Wind Tunnel. In Proceedings of the 20th Structures, Structural Dynamics, and Materials Conference, St. Louis, MO, USA, 4–6 April 1979. [CrossRef]
3. Herron, R.; Stich, P.; Price, E., Jr.; Whoric, J. Further Improvements in Cost Effectiveness of Wind Tunnel Testing at PWT. In Proceedings of the Advanced Measurement and Ground Testing Conference, New Orleans, LA, USA, 17–20 June 1996. [CrossRef]
4. Peters, W.; Lawrence, W.; Mills, M.; Milam, W. Cycle time reduction strategies and improvements in transonic testing in the AEDC Wind Tunnel 16T. In Proceedings of the 37th Aerospace Sciences Meeting and Exhibit, Reno, NV, USA, 11–14 January 1999. [CrossRef]
5. Xu, A.; Lin, H.; Fu, J.; Sun, W. Wind-resistant structural optimization of supertall buildings based on high-frequency force balance wind tunnel experiment. *Eng. Struct.* **2021**, *248*, 113247. [CrossRef]
6. Araujo-Estrada, S.A.; Lowenberg, M.H.; Neild, S.A. Capturing nonlinear time-dependent aircraft dynamics using a wind tunnel manoeuvre rig. *Aerosp. Sci. Technol.* **2022**, *121*, 107325. [CrossRef]
7. Ghazal, T.; Elshaer, A.; Aboshosha, H. Wind load evaluation on storm shelters using wind tunnel testing and North American design codes. *Eng. Struct.* **2022**, *254*, 113821. [CrossRef]
8. Brambilla, E.; Giappino, S.; Tomasini, G. Wind tunnel tests on railway vehicles in the presence of windbreaks: Influence of flow and geometric parameters on aerodynamic coefficients. *J. Wind Eng. Ind. Aerodyn.* **2022**, *220*, 104838. [CrossRef]
9. Zhang, W.; Xiao, Y.; Li, C.; Zheng, Q.; Tang, Y. Wind load investigation of self-supported lattice transmission tower based on wind tunnel tests. *Eng. Struct.* **2022**, *252*, 113575. [CrossRef]
10. Zhang, G.; Lan, L.; Wang, Y.; Nan, J.; Wan, X.; Wen, X.; Fu, Z.; Liu, Y.; Teng, Y. Wind tunnel experiments on the pollution characteristics of suspension insulators in an ion flow field. *J. Electrost.* **2022**, *115*, 103659. [CrossRef]

11. Aidoo, E.N.; Appiah, S.K.; Awashie, G.E.; Boateng, A.; Darko, G. Geographically weighted principal component analysis for characterising the spatial heterogeneity and connectivity of soil heavy metals in Kumasi, Ghana. *Heliyon* **2021**, *7*, e08039. [CrossRef]
12. Martinović, S.; Vlahović, M.; Vuksanović, M.; Glišić, D.; Volkov-Husović, T. Principal component analysis of morphological descriptors for monitoring surface defects induced by thermal shock. *J. Eur. Ceram. Soc.* **2021**, *41*, 423–429. [CrossRef]
13. Liu, Q.; Gui, Z.; Xiong, S.; Zhan, M. A principal component analysis dominance mechanism based many-objective scheduling optimization. *Appl. Soft Comput. J.* **2021**, *113*, 107931. [CrossRef]
14. Scharf, F.; Widmann, A.; Bonmassar, C.; Wetzel, N. A tutorial on the use of temporal principal component analysis in developmental ERP research—Opportunities and challenges. *Dev. Cogn. Neurosci.* **2020**, *54*, 101072. [CrossRef] [PubMed]
15. Liu, Z.; Han, H.-G.; Dong, L.-X.; Yang, H.-Y.; Qiao, J.-F. Intelligent decision method of sludge bulking using recursive kernel principal component analysis and Bayesian network. *Control Eng. Pract.* **2022**, *121*, 105038. [CrossRef]
16. Hao, W. Classification of Sport Actions Using Principal Component Analysis and Random Forest Based on Three-Dimensional Data. *Displays* **2021**, *72*, 102135. [CrossRef]
17. Jin, Q.; Wang, H. Principal component analysis for fractional quantum Hall states in bilayer systems. *Phys. Lett. A* **2022**, *427*, 127921. [CrossRef]
18. Sun, L.; Wang, K.; Xu, L.; Zhang, C.; Balezentis, T. A time-varying distance based interval-valued functional principal component analysis method—A case study of consumer price index. *Inf. Sci.* **2022**, *589*, 94–116. [CrossRef]
19. Gang, A.; Bajwa, W.U. A linearly convergent algorithm for distributed principal component analysis. *Signal Process.* **2022**, *193*, 108408. [CrossRef]
20. Han, Y.; Song, G.; Liu, F.; Geng, Z.; Ma, B.; Xu, W. Fault monitoring using novel adaptive kernel principal component analysis integrating grey relational analysis. *Process Saf. Environ. Prot.* **2022**, *157*, 397–410. [CrossRef]
21. Dunia, R.; Qin, S.J.; Edgar, T.F.; McAvoy, T.J. Identification of faulty sensors using principal component analysis. *AIChE J.* **1996**, *42*, 2797–2812. [CrossRef]
22. Wang, S.W.; Xiao, F. Sensor Fault Detection and Diagnosis of Air-Handling Units Using a Condition-Based Adaptive Statistical Method. *HVACR Res.* **2006**, *12*, 127–150. [CrossRef]
23. Hu, Y.; Chen, H.; Xie, J.; Yang, X.; Zhou, C. Chiller sensor fault detection using a self-Adaptive Principal Component Analysis method. *Energy Build.* **2012**, *54*, 252–258. [CrossRef]
24. Navi, M.; Davoodi, M.R.; Meskin, N. Sensor Fault Detection and Isolation of an Industrial Gas Turbine Using Partial Kernel PCA. *IFAC Pap.* **2015**, *48*, 1389–1396. [CrossRef]
25. Sharifi, R.; Langari, R. Nonlinear sensor fault diagnosis using mixture of probabilistic PCA models. *Mech. Syst. Signal Process.* **2017**, *85*, 638–650. [CrossRef]
26. Li, W.; Peng, M.; Wang, Q. Improved PCA method for sensor fault detection and isolation in a nuclear power plant. *Nucl. Eng. Technol.* **2019**, *51*, 146–154. [CrossRef]
27. Li, G.; Hu, Y. An enhanced PCA-based chiller sensor fault detection method using ensemble empirical mode decomposition based denoising. *Energy Build.* **2019**, *183*, 311–324. [CrossRef]
28. Yu, Y.; Peng, M.; Wang, H.; Ma, Z.; Li, W. Improved PCA model for multiple fault detection, isolation and reconstruction of sensors in nuclear power plant. *Ann. Nucl. Energy* **2020**, *148*, 107662. [CrossRef]
29. Zhu, S.; Xia, H.; Annor-Nyarko, M.; Yin, W.; Peng, B.; Wang, Z.; Zhang, J. A robust strategy for sensor fault detection in nuclear power plants based on principal component analysis. *Ann. Nucl. Energy* **2021**, *164*, 108621. [CrossRef]
30. Mohamed, L.; Ibrahim, A.S. Model-based fault diagnosis via parameter estimation using knowledge base and fuzzy logic approach. In Proceedings of the 11th IEEE Mediterranean Electrotechnical Conference, Cairo, Egypt, 7–9 May 2002. [CrossRef]
31. Berriri, H.; Slama-Belkhodja, I. Enhanced parity equations method for sensor fault detection in electrical drives. In Proceedings of the 2010 Conference on Control and Fault-Tolerant Systems (SysTol), Nice, France, 6–8 October 2010.
32. Langari, R. Isolability of faults in sensor fault diagnosis. *Mech. Syst. Signal Process.* **2011**, *25*, 2733–2744. [CrossRef]
33. Rao, A.R.M.; Kasireddy, V.; Gopalakrishnan, N.; Lakshmi, K. Sensor fault detection in structural health monitoring using null subspace–based approach. *J. Intell. Mater. Syst. Struct.* **2015**, *26*, 172–185. [CrossRef]
34. Li, Y.; Zhang, J.; Deng, F.; Chen, J. Sensor Fault Diagnosis based on On-line Random Forests. In Proceedings of the 2016 35th Chinese Control Conference (CCC), Chengdu, China, 27–29 July 2016. [CrossRef]
35. Shahnazi, R.; Zhao, Q. Adaptive Fuzzy Descriptor Sliding Mode Observer-based Sensor Fault Estimation for Uncertain Nonlinear Systems. *Asian J. Control* **2006**, *18*, 1478–1488. [CrossRef]
36. Li, Y.; Yang, T.; Jian, L.; Na, F.; Guan, W. A Fault Diagnosis Method by Multi Sensor Fusion for Spacecraft Control System Sensors. In Proceedings of the 2016 IEEE International Conference on Mechatronics and Automation, Harbin, China, 7–10 August 2016. [CrossRef]
37. Heydarzadeh, M.; Nourani, M. A Two-Stage Fault Detection and Isolation Platform for Industrial Systems Using Residual Evaluation. *IEEE Trans. Instrum. And Meas.* **2016**, *65*, 2424–2432. [CrossRef]
38. Tolouei, H.; Shoorehdeli, M.A. Nonlinear parity approach to sensor fault detection in pH neutralization system. In Proceedings of the 2017 25th Iranian Conference on Electrical Engineering (ICEE), Tehran, Iran, 2–4 May 2017; pp. 889–894. [CrossRef]
39. Kullaa, J. Sensor validation using minimum mean square error estimation. *Mech. Syst. Signal Process.* **2010**, *24*, 1444–1457. [CrossRef]

40. Kullaa, J. Distinguishing between sensor fault, structural damage, and environmental or operational effects in structural health monitoring. *Mech. Syst. Signal Process.* **2011**, *25*, 2976–2989. [CrossRef]
41. Kullaa, J. Detection, identification, and quantification of sensor fault in a sensor network. *Mech. Syst. Signal Process.* **2013**, *40*, 208–221. [CrossRef]
42. Kullaa, J.; Santaoja, K.; Anthony, E. Vibration-Based Structural Health Monitoring of a Simulated Beam with a Breathing Crack. *Key Eng. Mater.* **2013**, *569–570*, 1093–1100. [CrossRef]